Electron transport in quantum cascade lasers in a magnetic field

Ivana Savić* and Zoran Ikonić
School of Electronic and Electrical Engineering, University of Leeds, Leeds LS2 9JT, United Kingdom

Vitomir Milanović†
Faculty of Electrical Engineering, University of Belgrade, 11120 Belgrade, Serbia and Montenegro

Nenad Vukmirović, Vladimir D. Jovanović, Dragan Indjin, and Paul Harrison
School of Electronic and Electrical Engineering, University of Leeds, Leeds LS2 9JT, United Kingdom
(Received 17 October 2005; revised manuscript received 13 December 2005; published 17 February 2006)

A theoretical model of electron transport in quantum cascade lasers subjected to a magnetic field is developed. The Landau level electronic structure was calculated from the envelope-function Schrödinger equation within the effective-mass approximation. The electron transport in a magnetic field was modeled using the self-consistent rate-equation description for the full period of the cascade and its interaction with adjacent periods. The scattering processes included in the model are electron–longitudinal-optical-phonon, electron–longitudinal-acoustic-phonon, and electron-electron scattering. All these processes show oscillatory behavior with magnetic field, and their interplay determines the electron transport and the output characteristics of quantum cascade lasers in magnetic field. The model was applied to investigate the influence of magnetic field on the performance of a GaAs/AlGaAs quantum cascade laser emitting at $\lambda \approx 11.4$ μm [P. Kruck *et al.*, Appl. Phys. Lett. **76**, 3340 (2000)]. The calculated results show good overall agreement with the available experimental data.

DOI: 10.1103/PhysRevB.73.075321 PACS number(s): 73.63.Hs

I. INTRODUCTION

Quantum cascade lasers[1] (QCL's) based on GaAs/AlGaAs have undergone significant advances since their first realization.[2] Pulsed room-temperature operation has been reported in several midinfrared QCL's.[3,4] Also, continuous wave operation in the midinfrared region up to 150 K has been achieved.[5] QCL operation has been demonstrated in the far-infrared range up to 210 μm.[6–10] Recently, experimental observations of enhanced population inversion and reduced threshold current in QCL's in a magnetic field have been reported.[10–17] Previous theoretical work aiming to explain the influence of a magnetic field on the physical processes involved has been focused only on processes in the active region. Several studies have analyzed electron–longitudinal-optical (LO)-phonon scattering between the upper and lower laser levels in midinfrared QCL's,[12–14,18] and very few have considered electron-electron scattering between these levels in THz QCL's.[19] Modeling of the active region of QCL's, including electron-LO-phonon and electron–longitudinal-acoustic (LA)-phonon scattering, and assuming a unity injection approximation, has been reported.[20,21] However, none of these studies has investigated the electron transport through the injector-active region-collector cascade.

The influence of electron-electron scattering on QCL performance in a magnetic field may be significant, since it determines electron injection efficiency from the injector into the upper laser level.[22] Various parasitic mechanisms, such as leakage from the injector directly into the ground and lower laser levels, the continuum states, and the collector, degrade the population inversion and hence the optical gain. These effects cannot be investigated without consideration of the injector region and inclusion of electron-electron scattering into the model.

The aim of this work is to develop a comprehensive model of electron transport in QCL's in a magnetic field, considering full QCL periods (both the injector-collector and active regions). The main objective is to determine the electron populations and scattering rates between Landau levels in the structure and then to calculate the QCL output characteristics, such as the current density, the gain, and the threshold current. The results, together with a theoretical background, should provide a better insight into the underlying physical phenomena. Also, the model should enable the design of novel quantum cascade structures operating in magnetic field and prediction of their output characteristics. A detailed analysis is performed for a midinfrared GaAs/AlGaAs QCL in a magnetic field,[23] which has been studied experimentally.[13,14]

II. THEORETICAL CONSIDERATIONS

A. Electronic structure of quantum wells in a magnetic field

Application of a magnetic field perpendicular to quantum well layers splits the in-plane continuum of quantized subbands into Landau levels (LL's), additionally described by Landau and spin indices.[24] The electronic structure of quantum wells in a magnetic field is found by solving the Schrödinger equation for envelope functions using the effective-mass approximation.[25] The LL calculation accounts for the nonparabolicity of both the parallel and perpendicular effective masses.[26] Neglecting the spin splitting, the energy of the (j_i)th LL originated from the (m_i)th state (subband), with further considerations denoted with a shorthand subscript i, $i=|m_i,j_i\rangle$, is

$$E_i = E_{|m_i,j_i\rangle} = \bar{E}_{m_i} + \left(j_i + \frac{1}{2}\right)\frac{\hbar eB}{\bar{m}_{m_i\|}}, \quad (1)$$

where $\bar{E}_{m_i}$ is the energy of state m_i, $\hbar$ is Planck's constant, e is the electron charge, B is the applied magnetic field, $\bar{m}_{m_i\|}^{-1} = \int \bar{\psi}_{m_i}^2(z) m_\|^{-1}(z, \bar{E}_{m_i}) dz$, where $m_\|(z,E) = m^*(z)\{1 + (2\alpha' + \beta')\times[E - U(z)]\}$, is the parallel effective mass, $m^*(z)$ is the position-dependent band-edge electron effective mass, α' and β' are the nonparabolicity parameters, and $U(z)$ is the conduction band profile. Along the z axis, the wave functions of LL's are independent of their Landau index $[\psi_i(z) = \bar{\psi}_{m_i}(z)]$.

We should note that the decoupling between the motion perpendicular and parallel to the layers, characterized by the corresponding effective masses, is valid for infinite quantum wells[26] (QW's) and is a good approximation for finite QW's if they are not too narrow. Since QCL's comprise periods of relatively narrow, coupled QW's, this decoupling may be questionable. However, since a more rigorous consideration of this problem in such a complex structure is not trivial, the decoupling approximation was used for QCL's.

B. Interaction of electrons with an electromagnetic field

For z-polarized radiation optical transitions are allowed only between LL's of the same Landau and spin index, and all of them have the same value of the dipole matrix element. The optical gain is calculated considering transitions between all LL's stemming from the upper and lower laser levels[25,27,28] (denoted as states 4 and 2, respectively),

$$G_{4,2} = \frac{e^2\omega}{n\epsilon_0 c} M_{4,2}^2 \sum_{\substack{i,f \\ (m_i=4, m_f=2, j_i=j_f=j)}} (n_i - n_f) \times \frac{\gamma/2}{(E_i - E_f - \hbar\omega)^2 + (\gamma/2)^2}, \quad (2)$$

where $i = |m_i, j\rangle$ and $f = |m_f, j\rangle$ are LL's stemming from states $m_i = 4$ and $m_f = 2$ of the same Landau index j, E_i and E_f are their energies with the corresponding wave functions $\bar{\psi}_4$ and $\bar{\psi}_2$, $M_{4,2} = \int \bar{\psi}_4^*(z) z \bar{\psi}_2(z) dz$ is the dipole matrix element, n_i and n_f are the electron sheet densities, ω is the frequency of incident radiation, n is the refraction index, ϵ_0 is the permittivity of vacuum, c is the speed of light in vacuum, and γ is the transition linewidth [full width at half maximum (FWHM)].

C. Scattering processes

The present model includes electron–LO-phonon, electron–LA-phonon, and electron-electron scattering. Recent experimental results for structures with higher electron densities indicate that electron-electron scattering is more important than interface roughness and ionized impurity scattering.[29] It has been also suggested that at large magnetic fields and low temperatures the interface roughness and impurities do not lead to intersubband scattering but to an inhomogeneous broadening of the gain because of carrier localization.[10] Therefore, the latter two scattering processes are considered negligible.

The scattering processes in an external magnetic field may be significantly enhanced or suppressed, depending on the inter-LL energy separation. The electron–LO-phonon scattering between two LL's increases considerably as their energy difference approaches the resonant LO phonon energy ($\sim$36 meV in GaAs). A similar conclusion applies for electron-electron scattering, where a resonance occurs when the total energies of two initial and two final LL's are equal. Electron–LA-phonon scattering also shows resonant behavior when two LL's have very similar energies.

1. Interaction of electrons with longitudinal optical phonons

The electron–longitudinal-optical-phonon scattering rate between LL's $i = |m_i, j_i\rangle$ and $f = |m_f, j_f\rangle$ if $j_i \leqslant j_f$ reads[28]

$$W_{i,f} = \frac{e^2\omega_{\mathrm{LO}}}{2\pi\epsilon_p}\left[n_0(\omega_{\mathrm{LO}}) + \frac{1}{2} \mp \frac{1}{2}\right]\delta(E_i - E_f \pm \hbar\omega_{\mathrm{LO}}) \times \int_0^\infty q_{xy}|H_{j_i,j_f}(q_{xy})|^2\, \mathrm{d}q_{xy} \int_0^\infty \frac{|G_{m_i,m_f}(q_z)|^2}{q_{xy}^2 + q_z^2} dq_z, \quad (3)$$

where ω_{LO} is the optical phonon frequency, $\boldsymbol{q}_{xy}$ ($q_{xy} = |\boldsymbol{q}_{xy}|$) is the xy component and q_z is the z component of the phonon wave vector $\boldsymbol{q} = (\boldsymbol{q}_{xy}, q_z)$, the constant ϵ_p is defined as $\epsilon_p^{-1} = \epsilon_\infty^{-1} - \epsilon_s^{-1}$ where ϵ_∞ and ϵ_s are high-frequency and static permittivity, respectively, and $n_0(\omega_{\mathrm{LO}})$ is the Bose-Einstein factor. To calculate the scattering rate for $j_i > j_f$, one swaps the two subscripts. The upper sign in the $\left[n_0(\omega_{\mathrm{LO}}) + \frac{1}{2} \mp \frac{1}{2}\right]$ term and in the energy conservation law (the δ function) holds for absorption and the lower sign for emission.

The form factor $G_{m_i,m_f}(q_z)$ is defined as

$$G_{m_i,m_f}(q_z) = \int \bar{\psi}_{m_f}^*(z) e^{iq_z z} \bar{\psi}_{m_i}(z) dz. \quad (4)$$

The lateral overlap integral $H_{j_i,j_f}(q_{xy})$ is given in analytic form

$$|H_{j_i,j_f}(q_{xy})|^2 = e^{-q_{xy}^2/2\beta^2} \frac{j_i!}{j_f!}\left(\frac{q_{xy}^2}{2\beta^2}\right)^{j_f - j_i}\left[L_{j_f}^{j_f - j_i}\left(\frac{q_{xy}^2}{2\beta^2}\right)\right]^2, \quad (5)$$

where $\beta = \sqrt{m^*\omega_c/\hbar} = \sqrt{eB/\hbar}$ and $L_n^k(x)$ is the associated Laguerre polynomial. The δ function was replaced by a Gaussian distribution with the standard deviation given as $\sigma = \sigma_0\sqrt{B}$, where $\sigma_0 = 1$ meV/T$^{1/2}$,[30] to account for state broadening.

2. Interaction of electrons with longitudinal acoustical phonons

The transition of an electron from the ith LL ($i = |m_i, j_i\rangle$) with larger energy than that of the final fth LL ($f = |m_f, j_f\rangle$) via an interaction with longitudinal acoustic phonons in a magnetic field is given by[28]

$$W_{i,f} = \frac{D_A^2 (E_i - E_f)^2}{\pi \rho v_s^4 \hbar^3} \frac{e^{(E_i - E_f)/kT}}{e^{(E_i - E_f)/kT} - 1} \times \int_0^{q_{z\max}} |G_{m_i,m_f}(q_z)|^2 |H_{j_i,j_f}(q_{xy0})|^2 dq_z, \quad (6)$$

where

$$q_{xy0} = \sqrt{\left(\frac{E_i - E_f}{\hbar v_s}\right)^2 - q_z^2}. \quad (7)$$

Here D_A is the deformation potential, ρ is the density of the material, v_s the sound velocity, $G_{m_i,m_f}(q_z)$ and $H_{j_i,j_f}(q_{xy})$ are the form factor and the lateral overlap integral for electron–LO-phonon scattering, respectively, and

$$q_{z\max} = \frac{|E_i - E_f|}{\hbar v_s}. \quad (8)$$

If $E_i < E_f$, the electron-LA scattering is calculated from a similar expression

$$W_{i,f} = \frac{D_A^2 (E_i - E_f)^2}{\pi \rho v_s^4 \hbar^3} \frac{1}{e^{(E_i - E_f)/kT} - 1} \times \int_0^{q_{z\max}} |G_{m_i,m_f}(q_z)|^2 |H_{j_i,j_f}(q_{xy0})|^2 dq_z. \quad (9)$$

3. Electron-electron interaction

The electron-electron scattering rate from an initial state containing an electron in LL i with a wave vector k_i and an electron in LL j to a final state containing electrons in LL's f and g is[19,29]

$$W_{i,j,f,g}(k_i) = \frac{e^4}{8\pi^3 \epsilon_s^2 \hbar} \int\int M^2(k_i,k_j,k_f) dk_j dk_f \times \delta(E_f + E_g - E_i - E_j), \quad (10)$$

where k_i, k_j, and k_f are the electron wave vectors of LL's i, j, and f, respectively. The scattering matrix element is given as

$$M(k_i,k_j,k_f) = \int\int u_{j_f}^*(x - f(k_f)) u_{j_g}^*(x' - f(k_g)) \times u_{j_i}(x - f(k_i)) u_{j_j}(x' - f(k_j)) dx\, dx' \times \int\int \bar{\psi}_{m_f}^*(z) \bar{\psi}_{m_g}^*(z') \bar{\psi}_{m_i}(z) \bar{\psi}_{m_j}(z') \times K_0[|k_f - k_i| \sqrt{(x - x')^2 + (z - z')^2}] dz\, dz', \quad (11)$$

where $u_{j_i}(x - f(k_i))$ is the harmonic oscillator wave function of LL i, $f(k_i) = k_i/(eB/\hbar)$, K_0 is a modified Bessel function of the second kind, and k_g is the electron wave vector of LL g, equal to $k_i + k_j - k_f$. No screening appears in this expression.[19,29] A Gaussian of the same standard deviation as in the electron–LO-phonon scattering was used instead of the δ function to model LL broadening.

D. Electron transport in a cascade

A semiclassical model of electron dynamics in QCL's in a magnetic field is developed in order to describe the electron transport processes. The populations of LL's in a QCL with a large number of periods in an electric and magnetic field are obtained from the system of rate equations in the steady state[28,31]:

$$\frac{dn_f}{dt} = 0 = \sum_i n_i W_{i,f}(1 - \alpha_B n_f) - n_f \sum_i W_{f,i}(1 - \alpha_B n_i) + \sum_{i,j,g} n_i W_{i,j,f,g} \alpha_B n_j (1 - \alpha_B n_f)(1 - \alpha_B n_g) - n_f \sum_{i,j,g} W_{f,g,i,j} \alpha_B n_g (1 - \alpha_B n_i)(1 - \alpha_B n_j), \quad (12)$$

where i, j, f, and g run over all LL's in the cascade, in all of its periods, n_i is the electron concentration in ith LL, $W_{i,f}$ is the scattering rate from LL i into LL f, and $W_{i,j,f,g}$ is the two-electron scattering rate from LL's i and j into LL's f and g, both independent of the electron distribution. The electron-electron scattering rate $W_{i,j,f,g}$ is calculated by averaging Eq. (10) over the initial wave vector k_i. The Pauli exclusion principle, usually embedded in the total scattering rate expressions, is extracted in form of the factors $\alpha_B n_i$ and $(1 - \alpha_B n_i)$, where $\alpha_B = \pi\hbar/eB$.

The periodicity of the QCL design enables solving the system of rate equations in a similar manner as proposed in Ref. 32. Each state and its LL's can be associated with one of the periods of the QCL due to the wave-function localization properties. Then, the tight-binding description can be introduced by accounting for several neighboring periods. A globally linear variation of the conduction band potential is assumed. Therefore, each period has an identical set of N LL's, with identical electron distributions ($n_i = n_{i+kN}$, $k = 0, \pm 1, \pm 2, \ldots$) and identical scattering rates ($W_{i,j} = W_{i+kN,j+kN}$). Their wave functions are replicas of each other, translated in space and energy. Then, the system of rate equations takes a simplified form

$$\frac{dn_f}{dt} = 0 = \sum_{k=-P}^{P} \sum_{i=1}^{N} n_i W_{i+kN,f}(1 - \alpha_B n_f) - n_f \sum_{k=-P}^{P} \sum_{i=1}^{N} W_{f,i+kN}(1 - \alpha_B n_i) + \sum_{\substack{k,k',k''=-P \\ (|\Delta k| \le P)}}^{P} \left[\sum_{i,j,g=1}^{N} n_i W_{i+kN,j+k'N,f,g+k''N} \alpha_B \times n_j (1 - \alpha_B n_f)(1 - \alpha_B n_g) - n_f \sum_{i,j,g=1}^{N} W_{f,g+k''N,i+kN,j+k'N} \alpha_B n_g (1 - \alpha_B n_i)(1 - \alpha_B n_j) \right], \quad (13)$$

where i, j, f, and g now run over all LL's assigned to one period and P is the number of its adjacent periods on each side. Furthermore, using the translation invariance of scatter-

ing rates ($W_{i-kN,j}=W_{i,j+kN}$), the rate equations may be written so as to contain only the scattering rates with positive subscripts. $N-1$ out of the total of N equations are linearly independent. Therefore, if solving them as a set of nonlinear equations to find the steady-state solution, one rate equation should be replaced by the electroneutrality condition. On the other hand, if calculating the time evolution of Eq. (13), this comes in as the set of initial conditions.

The current density is calculated by accounting for all the components due to electron scattering through some reference plane—e.g., the interface between the central period and the adjacent right period:

$$J = \sum_{\substack{k,k'=-P \\ (|\Delta k| \leqslant P)}}^{P} \sum_{i,f=1}^{N} n_i W_{i+kN,f+k'N}(1-\alpha_B n_f)[h(k')-h(k)]$$
$$+ \sum_{\substack{k,k',k'',k'''=-P \\ (|\Delta k| \leqslant P)}}^{P} \sum_{i,j,f,g=1}^{N} n_i W_{i+kN,j+k'N,f+k''N,g+k'''N}\alpha_B n_j(1-\alpha_B n_f)$$
$$\times(1-\alpha_B n_f)(1-\alpha_B n_g)[h(k'')+h(k''')-h(k)-h(k')], \tag{14}$$

where $h(k)=1$ if $k\in[1,P]$ and $h(k)=0$ if $k\in[-P,0]$. In the example considered below, all the states are reasonably well located in the period they are assigned to, so we use the scattering between the nearest-neighbor periods only; i.e., we set $P=1$ in the above expressions.

We should note that there is no temperature, except the lattice temperature, which appears in this model. That is, no particular form of electron distribution is assigned to the set of LL's associated with one size-quantized state, which all "originate" from different in-plane wave vectors existing in the zero field limit. In contrast, the electron distribution over all, fully discrete, levels is found from the above rate equations. Despite the name, therefore, the model corresponds to the Boltzmann-equation rather than the rate-equation approach, in the terminology used (for the zero-field case) in the QCL community, and the type of "thermal self-consistency" it achieves corresponds to that obtained, e.g., in Monte Carlo simulations of QCL's in zero magnetic field.[32]

A consequence of this level of detail is that a considerably larger number of levels (typically ~200) is handled than is usual in the rate-equation model of QCL's at zero field. Solving a system of nonlinear equations of that size becomes difficult when using conventional, gradient-based methods, because they frequently fail to converge. In order to find the stationary solution of Eq. (13) we actually track the time evolution of nonstationary rate equations: starting with an arbitrary (but reasonable) initial guess, the rate equations are integrated in time until the distribution becomes essentially stationary. Although perhaps not the fastest, this method proved to be extremely reliable in terms of convergence.

Upon obtaining electron populations from the self-consistent rate equations (local self-consistency), their contribution to the effective conduction band potential can be calculated from the Poisson equation, completing one iteration of the globally self-consistent calculation. Iterations should be performed until convergence of the conduction band profile, and hence the electronic structure and electron populations, is reached. However, in this work, the computational time of a single iteration is too large to enable the realization of the entire globally self-consistent process. Only one iteration was performed, and the change of energy spacing between any two states was always less than 10%.

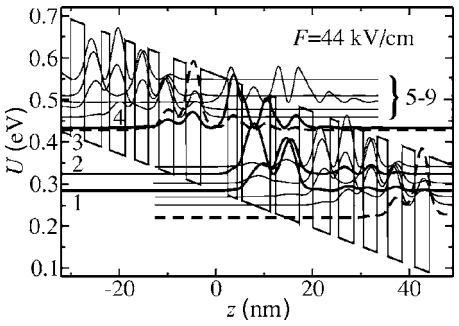

FIG. 1. A schematic diagram of the conduction band profile, energy levels, and squared wave functions for an injector-active region-collector section of the ~11.4-μm GaAs/$Al_{0.33}Ga_{0.67}As$ QCL for an applied electric field of 44 kV/cm. The active region levels are shown in bold and denoted as 1, 2, and 4, respectively. The first injector state is represented by dashed lines and denoted as 3. Other injector states are denoted as 5, 6, 8, and 9. State 7 represents a continuumlike state.

III. NUMERICAL RESULTS AND DISCUSSION

The calculation and analysis of the electron transport were performed for the ~11.4−μm GaAs/$Al_{0.33}Ga_{0.67}As$ QCL, described in Refs. 13 and 14, similar to the QCL from Ref. 23. The electric field was set to 44 kV/cm, the value for which this QCL achieves threshold in zero magnetic field. The lattice temperature was set to 4 K, and the magnetic field was varied between 10 T and 60 T, as in the experiment.[14] The calculation can be performed for magnetic field less than 10 T, though it becomes extremely time consuming due to the increasing number of relevant LL's as the magnetic field decreases. Furthermore, for small magnetic fields the broadening of LL's becomes larger than the inter-LL separation and the magnetic field does not affect the transport. Therefore, a zero-field calculation[22,31] appears to be more appropriate for the weak-field limit. The electronic structure of the QCL at zero magnetic field is illustrated in Fig. 1. The active region levels 1, 2, and 4 represent the ground, the lower, and the upper laser levels, respectively. The injector-collector states are denoted as 3, 5, 6, 8, and 9. State 7 represents a weakly localized continuumlike state.

A. Electron population

The calculated populations of LL's associated with the active region levels and the first injector state, as functions of magnetic field, are given in Fig. 2. To emphasize the importance of including electron-electron scattering in the model, the results obtained without this scattering mechanism are shown in Fig. 3. Comparison of the two figures clearly

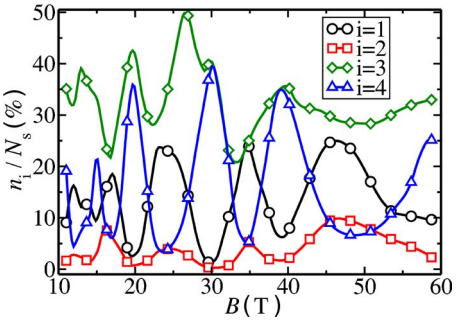

FIG. 2. (Color online) The electron distribution over QCL states (all Landau levels) vs magnetic field, calculated with electron-electron scattering included. States 1, 2, 3, and 4 represent the ground state, the lower laser level, the first injector state, and the upper laser level, respectively. N_S is the total sheet density of electrons per period.

shows that neglecting electron-electron scattering in the model leads to different electron distributions, especially of the upper laser level and the first injector state, and hence also to incorrect estimate of the output characteristics.

For some values of the magnetic field (18–22 T, 28–32 T, 38–42 T), the population of the upper laser level almost equals the population of the first injector state (see Fig. 2), while the other states are depopulated. The same situation occurs in QCL's without a magnetic field when the electric field is increased above threshold. For other values of the magnetic field, the population of the upper laser level is considerably smaller than that of the first injector state, while the populations of all other states are increased.

The population of higher injector states and the lower laser level are low throughout the magnetic field range considered. It is only the populations of the second injector state for $B \leqslant 20$ T and of the third injector state for $B > 20$ T that have significant values, suggesting their major contribution in the extraction of electrons from the ground state.

It is interesting to look into the electron distributions over LL's stemming from different states. This is shown in Fig. 4 for two different magnetic fields. With the exception of the first injector state, these distributions do not appear to be

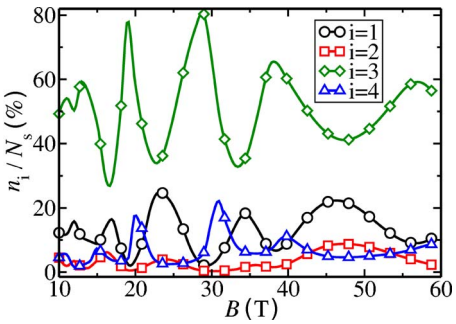

FIG. 3. (Color online) The electron distribution over QCL states (all Landau levels) vs magnetic field, calculated with electron-electron scattering neglected. States 1, 2, 3, and 4 represent the ground state, the lower laser level, the first injector state, and the upper laser level, respectively. N_S is the total sheet density of electrons per period.

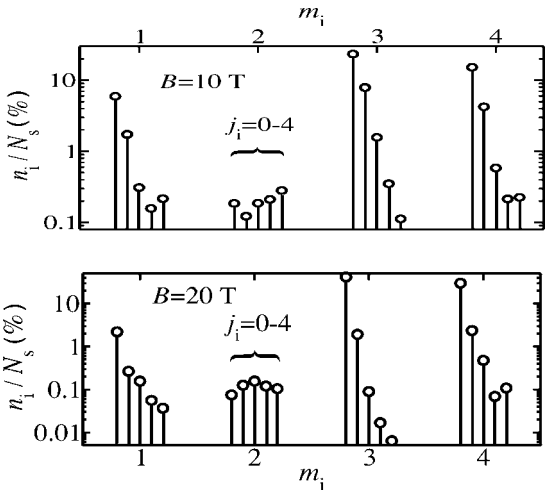

FIG. 4. The electron distribution over first five Landau levels stemming from the first four QCL states for magnetic fields of 10 T (upper pane) and 20 T (lower pane). States 1, 2, 3, and 4 represent the ground state, the lower laser level, the first injector state, and the upper laser level, respectively.

very well thermalized (the lower laser level being the most remote from it) and the general shape of distributions changes with the field. The first injector state is almost completely thermalized, and an effective electron temperature of 140 K at $B=10$ T and 154 K at $B=20$ T can be extracted from Fig. 4. Had all the distributions been found to be thermalized, this would indicate the possibility to reduce the order of the model by defining the averaged-over-LL's scattering rates between size-quantized states, in the same manner as is done in the rate equations model of QCL's at zero field (in which case the effective-state temperatures would appear, to be determined from energy balance considerations). However, electron-electron scattering is not fast enough to create such conditions, at least not in the structure considered here, and this requires the use of the present model.

B. Scattering rates

The transition rates between LL's determine the LL population and the current across the device, particularly the transitions between LL's stemming from the first injector state and the active region and from the upper and lower laser levels. Therefore, we discuss them in some more detail.

The average scattering rate between the LL's originating from state m_i into the LL's originating from state m_f is defined as

$$W^a_{m_i m_f} = \frac{\sum_{j_i} \sum_{j_f} n_{|m_i,j_i\rangle} W_{|m_i,j_i\rangle,|m_f,j_f\rangle}}{\sum_{j_i} n_{|m_i,j_i\rangle}}. \tag{15}$$

The total average scattering rate from the LL's associated with state m_i into the LL's associated with any other state $m_f \neq m_i$ is then defined as

$$W^a_{m_i} = \sum_{m_f \neq m_i} W^a_{m_i m_f}. \tag{16}$$

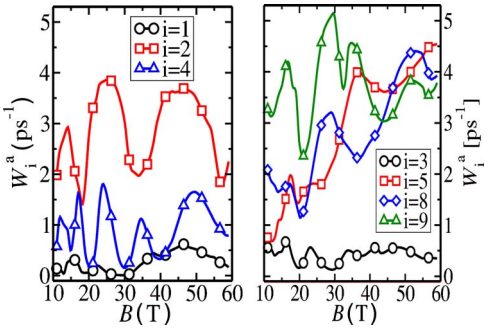

FIG. 5. (Color online) Left: total average scattering rates (see text for explanation) from the active region levels (all Landau levels) vs magnetic field. States 1, 2, and 4 represent the ground state, the lower laser level, and the upper laser level, respectively. Right: total average scattering rates from the injector states (all Landau levels) vs magnetic field. States 3, 5, 8, and 9 represent first, second, fourth, and fifth injector states, respectively.

The total average scattering rates from LL's associated with each state are oscillatory functions of magnetic field (shown in Fig. 5), whose peaks are determined by resonances with the LL's of the other states. The calculation showed that electron–LO-phonon scattering is dominant for electron transfer in the active region and from the injector to the lower laser levels (the ground state + the lower laser level), while electron-electron scattering prevails for transfers within the injector, from the injector to the upper laser and continuum levels, and from the lower laser levels to the collector. The scattering rates of the first injector state and the ground state are the lowest scattering rates throughout the whole magnetic field range. The large values of scattering rates of other injector states imply fast relaxation in the injector. Efficient extraction from the lower laser level is enabled by its large scattering rate.

The average scattering rates from either the first injector state or the upper laser level into the lower laser levels are determined by electron–LO-phonon interactions and show prominent oscillations with magnetic field ($W^a_{3(1,2)}$ and $W^a_{4(1,2)}$ in Fig. 6). Each average scattering rate between LL's originating from two different states (W^a_{31}, W^a_{32}, W^a_{41}, W^a_{42}) exhibits a monotonic increase of peak values with magnetic

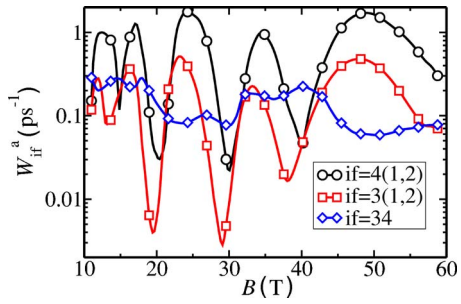

FIG. 6. (Color online) Average scattering rates (see text for explanation) from the first injector state (state 3) and the upper laser level (state 4) Landau levels into the lower laser level (states 1 and 2) Landau levels and from the first injector state to the upper laser level Landau levels vs magnetic field.

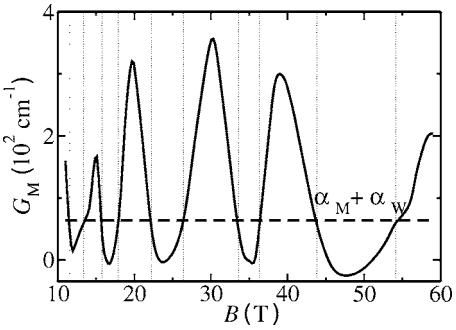

FIG. 7. Modal gain vs magnetic field dependence.

field, due to the increasing density of states of LL's.[18,19] Also, the peak-to-valley ratio increases and the valley values decrease, as a consequence of increasing separation between the resonances.[19] From Fig. 5, one can see that the peak and valley values of $W^a_{3(1,2)}=W^a_{31}+W^a_{32}$ and $W^a_{4(1,2)}=W^a_{41}+W^a_{42}$ show the same behavior up to 30 T.

Since the separation between the first injector state and the upper laser level is small (~5 meV), scattering between them is determined by the electron-electron interaction and electron–LO-phonon scattering is negligible. Furthermore, this energy separation is such that resonances between these states do not occur in the magnetic field range considered, so the oscillations of the scattering rate are not so pronounced. Its weak decreasing dependence on the magnetic field is attributed to the reduced electron-electron scattering cross section.[29]

C. Population inversion

The population inversion and, hence, the optical gain are determined by transitions between the first injector state and the active region and transitions between the upper and lower laser levels. If the electron-electron scattering from the first injector state into the upper laser level W^a_{34} is larger than the electron–LO-phonon scattering from the first injector state into the lower laser levels $W^a_{3(1,2)}$, the majority of electrons are injected into the upper laser level. A suppressed electron–LO-phonon scattering from the upper to the lower laser levels $W^a_{4(1,2)}$ leads to an enhanced population inversion (for magnetic fields of ≈11 T, 14–15 T, 18–22 T, 28–33 T, 37–42 T; see Fig. 7), and vice versa (12–14 T, 17–18 T, 26–28 T, 35–37 T, 42–43 T). If the electron–LO-phonon scattering from the first injector state to the lower laser levels $W_{3(1,2)}$ is dominant, the population inversion is insignificant or cannot be achieved, because of low injection into the upper laser level (≈12 T, 15–17 T, 22–26 T, 33–35 T, 43–56 T). For magnetic fields of 56–60 T, when $W^a_{3,(1,2)} \approx W^a_{3,4}$, the population inversion can be obtained, due to sufficient injection into the upper laser level and rapid extraction of electrons from the lower laser level into the ground state.

D. Optical gain

Oscillations of population inversion with magnetic field translate into oscillations of the optical gain (Fig. 7), which

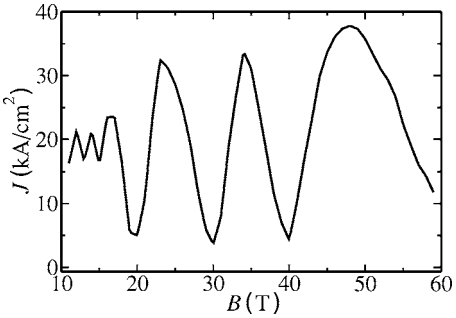

FIG. 8. Current density vs magnetic field dependence.

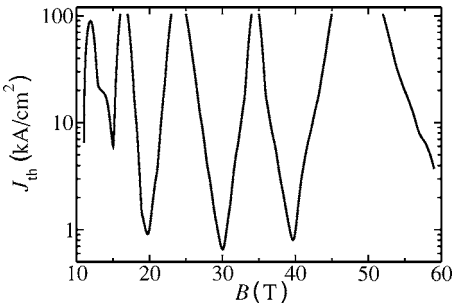

FIG. 9. Threshold current density vs magnetic field dependence.

reaches large peak values. The modal gain G_M is defined as $G_M = G_{4,2}\Gamma / L_p$, where Γ is the overlap factor between the optical mode and the core active region of the QCL [here $\Gamma = 0.36$ (Ref. 23)] and L_p is the length of one period. It was computed using the experimental value of the electroluminescence spectral width of 12.5 meV (Ref. 13) as the transition linewidth γ. It was assumed that the transition linewidth was independent of magnetic field, since such experimental data are not available, although a more accurate calculation should include this dependence. It was also assumed that the waveguide losses were independent of magnetic field, and the experimentally obtained mirror $\alpha_M = 19.5\ \mathrm{cm}^{-1}$ and waveguide $\alpha_W = 44\ \mathrm{cm}^{-1}$ losses for zero magnetic field[23] were used in the calculation. From the intersection points of the total loss line $\alpha_M + \alpha_W = 63.5\ \mathrm{cm}^{-1}$ and the $G_M(B)$ curve, we obtain the range of magnetic fields where lasing occurs, which is in fairly good agreement with measurements of the light intensity at threshold.[13] The calculated modal gain shows a similar trend as the light intensity, shown in Fig. 2 in Ref. 13. The disagreement between the results from the calculation and the experiment in the range 30–40 T is due to the approximate calculation of the electronic structure given in Sec. II A.

E. Current

The current is determined by transitions from the first injector state into the active region. The current versus magnetic field dependence is shown in Fig. 8. When the electron-electron scattering from the first injector state into the upper laser level W^a_{34} is larger than electron–LO-phonon scattering into the lower laser levels $W^a_{3(1,2)}$, the current is essentially determined by this electron-electron scattering, followed by the electron–LO-phonon scattering from the upper to the lower laser levels $W^a_{4(1,2)}$. Otherwise, the current is governed by the electron–LO-phonon scattering from the first injector state into the lower laser levels $W^a_{3(1,2)}$. Therefore, the magnetic field redirects the current through different transport channels, enhancing parasitic leakage from the injector into the lower laser levels when lasing is suppressed. The current density is characterized by increasing peak and decreasing valley values with increasing magnetic field, similar to the behavior of relevant scattering rates.

F. Threshold current

The exact calculation of the threshold current in a magnetic field requires the calculation of the current density versus electric field dependence, then modal gain versus current dependence, and finally, extraction of the threshold current J_{th} from $G_M(J_{th}) = \alpha_M + \alpha_W$, for each value of the magnetic field. Instead, we used an approximate expression $J_{th} = (\alpha_M + \alpha_W)/g\Gamma$, where g is the gain coefficient, after Ref. 33. Assuming a linear dependence of the modal gain on the current density $G_M = g\Gamma J$ when inversion is achieved (i.e., when G_M is positive), we get $J_{th} = J(\alpha_M + \alpha_W)/G_M$. For negative G_M, there is no lasing and the threshold current cannot be calculated within this approximation. Although this might be a rather crude approximation, it had to be adopted because each single bias-field combination requires a lot of computational time. The threshold current density dependence of the magnetic field is shown in Fig. 9. Its minima generally decrease with magnetic field and are constantly lower than the measured threshold current $6.6\ \mathrm{kA/cm}^2$ at zero magnetic field.[23] This is in qualitative agreement with the results from recent measurements of THz QCL's in magnetic fields.[10,17]

IV. CONCLUSION

A semiclassical model of electron transport in QCL's in a magnetic field was presented and used to analyze the operation of midinfrared GaAs/AlGaAs QCL's. We have calculated all relevant scattering rates, have shown their oscillatory dependence on magnetic field, and have discussed their influence on the electron transport. A significant contribution of electron-electron scattering to low-energy relaxation processes, particularly to injection into the upper laser level, was found. Large oscillations of the laser gain and redirection of current flow through different transport channels with magnetic field were observed. The calculated output characteristics are in good quantitative and qualitative agreement with the available experimental results.

ACKNOWLEDGMENTS

The authors would like to thank the European Office of Aerospace Research and Development for financial support under Contract No. FA8655-04-1-3069. The authors would also like to acknowledge discussions with O. Drachenko and D. Smirnov.

*Electronic address: eenis@leeds.ac.uk
†Also at School of Electronic and Electrical Engineering, University of Leeds, Leeds LS2 9JT, UK.

[1] J. Faist, F. Capasso, D. L. Sivco, C. Sirtori, A. L. Hutchinson, and A. Y. Cho, Science **264**, 553 (1994).
[2] C. Sirtori, P. Kruck, S. Barbieri, P. Collot, J. Nagle, M. Beck, J. Faist, and U. Oesterle, Appl. Phys. Lett. **73**, 3486 (1998).
[3] H. Page, C. Becker, A. Robertson, G. Glastre, V. Ortiz, and C. Sirtori, Appl. Phys. Lett. **78**, 3529 (2001).
[4] C. Pflügl, W. Schrenk, S. Anders, G. Strasser, C. Becker, C. Sirtori, Y. Bonetti, and A. Muller, Appl. Phys. Lett. **83**, 4698 (2003).
[5] H. Page, S. Dhillon, M. Calligaro, C. Becker, V. Ortiz, and C. Sirtori, IEEE J. Quantum Electron. **40**, 665 (2004).
[6] R. Köhler, A. Tredicucci, F. Beltram, H. E. Beere, E. H. Linfield, A. G. Davies, D. A. Ritchie, R. C. Iotti, and F. Rossi, Nature (London) **417**, 156 (2002).
[7] M. Rochat, L. Ajili, H. Willenberg, J. Faist, H. E. Beere, A. G. Davies, E. H. Linfield, and D. A. Ritchie, Appl. Phys. Lett. **81**, 1381 (2002).
[8] B. S. Williams, H. Callebaut, S. Kumar, Q. Hu, and J. Reno, Appl. Phys. Lett. **82**, 1015 (2002).
[9] G. Scalari, L. Sirigu, C. Walther, J. Faist, H. Beere, and D. Ritchie (unpublished).
[10] G. Scalari, S. Blaser, J. Faist, H. Beere, E. Linfield, D. Ritchie, and G. Davies, Phys. Rev. Lett. **93**, 237403 (2004).
[11] J. Ulrich, R. Zobl, K. Unterrainer, G. Strasser, and E. Gornik, Appl. Phys. Lett. **76**, 19 (2000).
[12] C. Becker, C. Sirtori, O. Drachenko, V. Rylkov, D. Smirnov, and J. Leontin, Appl. Phys. Lett. **81**, 2941 (2002).
[13] D. Smirnov, C. Becker, O. Drachenko, V. V. Rylkov, H. Page, J. Leotin, and C. Sirtori, Phys. Rev. B **66**, 121305(R) (2002).
[14] D. Smirnov, O. Drachenko, J. Leotin, H. Page, C. Becker, C. Sirtori, V. Apalkov, and T. Chakraborty, Phys. Rev. B **66**, 125317 (2002).
[15] G. Scalari, S. Blaser, L. Ajili, J. Faist, H. Beere, E. H. Linfield, D. Ritchie, and G. Davies, Appl. Phys. Lett. **83**, 3453 (2003).
[16] V. Tamosiunas, R. Zobl, J. Ulrich, K. Unterrainer, R. Colombelli, C. Gmachl, K. West, L. Pfeiffer, and F. Capasso, Appl. Phys. Lett. **83**, 3873 (2003).
[17] J. Alton, S. Barbieri, J. Fowler, H. E. Beere, J. Muscat, E. H. Linfield, D. A. Ritchie, G. Davies, R. Köhler, and A. Tredicucci, Phys. Rev. B **68**, 081303(R) (2003).
[18] C. Becker, A. Vasanelli, C. Sirtori, and G. Bastard, Phys. Rev. B **69**, 115328 (2004).
[19] K. Kempa, Y. Zhou, J. R. Engelbrecht, P. Bakshi, H. I. Ha, J. Moser, M. J. Naughton, J. Ulrich, G. Strasser, E. Gornik, and K. Unterrainer, Phys. Rev. Lett. **88**, 226803 (2002).
[20] I. Savić, P. Harrison, V. Milanović, D. Indjin, Z. Ikonić, and V. D. Jovanović, Phys. Status Solidi B **242**, 1812 (2005).
[21] J. Radovanović, V. Milanović, Z. Ikonić, D. Indjin, and P. Harrison, J. Appl. Phys. **97**, 103109 (2005).
[22] D. Indjin, P. Harrison, R. W. Kelsall, and Z. Ikonić, J. Appl. Phys. **91**, 9019 (2002).
[23] P. Kruck, H. Page, C. Sirtori, S. Barbieri, M. Stellmacher, and J. Nagle, Appl. Phys. Lett. **76**, 3340 (2000).
[24] L. D. Landau and E. M. Lifshitz, *Quantum Mechanics: Nonrelativistic Theory* (Pergamon, London, 1959).
[25] I. Savić, V. Milanović, Z. Ikonić, D. Indjin, V. Jovanović, and P. Harrison, IEEE J. Quantum Electron. **40**, 1614 (2004).
[26] U. Ekenberg, Phys. Rev. B **40**, 7714 (1989).
[27] S. Živanović, V. Milanović, and Z. Ikonić, Phys. Rev. B **52**, 8305 (1995).
[28] I. Savić, V. Milanović, N. Vukmirović, V. D. Jovanović, Z. Ikonić, D. Indjin, and P. Harrison, J. Appl. Phys. **98**, 084509 (2005).
[29] K. Kempa, Y. Zhou, J. R. Engelbrecht, and P. Bakshi, Phys. Rev. B **68**, 085302 (2003).
[30] J. P. Eisenstein, H. L. Stormer, V. Narayanamurti, A. Y. Cho, A. C. Gossard, and C. W. Tu, Phys. Rev. Lett. **55**, 875 (1985).
[31] Z. Ikonić, P. Harrison, and R. W. Kelsall, J. Appl. Phys. **96**, 6803 (2004).
[32] R. C. Iotti and F. Rossi, Phys. Rev. Lett. **87**, 146603 (2001).
[33] C. Sirtori, J. Faist, F. Capasso, D. L. Sivco, A. L. Hutchinson, and A. Y. Cho, IEEE J. Quantum Electron. **33**, 89 (1997).